Importance of matrix correlations in dye-doped solid rare gases: A hole-burning study

P. Geissinger,* L. Kador, and D. Haarer
Institute of Physics and "Bayreuther Institut für Makromolekülforschung (BIMF)," University of Bayreuth, D-95440 Bayreuth, Germany
(Received 28 July 1995; revised manuscript received 17 November 1995)

The present investigation was motivated by the apparent success of a statistical model to describe the effects of external pressure on spectral holes in dye-doped amorphous polymers. With its help, the polymer compressibility could be determined in a purely optical experiment. This success was surprising since polymers usually meet the basic assumptions of this model quite poorly. Furthermore, two conflicting approximations with respect to the number density of matrix units were employed. To investigate the model and its assumptions in a systematic way, we performed pressure-tuning experiments on spectral holes burnt in dye-doped rare-gas matrices, since these serve as simple model systems, satisfying the assumptions of the model to a large extent. A modification of the statistical theory to avoid the above-mentioned conflicting approximations by taking into account correlations between matrix units due to their mutual steric exclusion was extended further to also describe the pressure effects. The depth of the dye-matrix interaction potential and the number density of matrix units were calculated with and without correlations between matrix units. Our results provide experimental evidence that the inclusion of matrix correlations is essential to obtain reasonable potential parameters and number densities of the matrix atoms. The optically determined compressibilities, however, do not change upon introduction of matrix correlations. This result justifies earlier compressibility determinations using the original model.

I. INTRODUCTION

Polyatomic organic dye molecules can be investigated rather easily when they are doped into suitable solid host matrices in low concentrations. Due to the weak guest-host interaction, the electronic states of the guest molecule under study are largely decoupled from the host material, leaving the guest excitation energies localized. Therefore, the guest molecule will exhibit its characteristic electronic and vibronic splittings, except for a possible shift of the zero-phonon origin. The hosts are chosen such that their absorption does not overlap with the guest states under investigation. This holds true for a variety of polymers as well as *n*-alkanes and certainly for rare-gas matrices. In these cases, the low-energy optical absorption spectra of the guest-host systems are dominated by the respective guest molecules.

In disordered host materials the optical absorption spectra of these guest-host systems are often characterized by broad featureless bands. The reason for the featureless bands is the well-known inhomogeneous broadening. When a dye molecule is incorporated into a host matrix its transition energy will experience a shift due to the dye-matrix interaction. In a (hypothetic) perfect crystal, all guest molecules would experience exactly the same shift, whereas in disordered hosts, a distribution of local environments and therefore a distribution of transition energies is encountered. Hence, the inhomogeneous broadening, which can be as large as several 100 cm^{-1}, can serve as a measure of local disorder. On the other hand, the inhomogeneous broadening prevents access to the homogeneous absorption line shapes. The homogeneous linewidth is related to energy and phase relaxation processes in the system. Of particular interest are the linewidths in amorphous hosts, since in these materials additional low-energy excitations are present (TLS—two-level tunneling systems, local modes), which do not exist in crystals. The dye molecule therefore serves as a local probe of dynamical processes in disordered media via its homogeneous absorption line shape and linewidth.

With the introduction of hole-burning spectroscopy,[1,2] a method to extract homogeneous line shapes from inhomogeneously broadended absorption bands became available (for a review see, e.g., Ref. 3). A subensemble of molecules at a given frequency within the inhomogeneous band is selectively excited and subsequently phototransformed. If the product of the photoreaction absorbs at a different region in the spectrum, a dip in the original band—a spectral hole—will be left behind. Depending on the nature of the phototransformation, hole lifetimes can be as long as years. The hole width can then be linked to the homogeneous or quasi-homogeneous width of the transition. (Both widths differ by a factor of two in the case of shallow holes and in the absence of spectral diffusion.[4])

The enormous gain in resolution of the hole-burning technique also manifests itself in optical pressure-tuning experiments. Whereas pressure changes as high as several GPa are necessary to affect the whole inhomogeneous band shape, only a very small fraction (10^{-4}–10^{-5}) of the above-mentioned values are needed to give rise to measurable changes in the hole spectrum. This allows the investigation of pressure effects near equilibrium conditions. A pressure change Δp will cause a spectral hole to shift (linear in Δp) and to broaden (proportional to $|\Delta p|$). The hole shift is a consequence of the pressure-induced displacements of the matrix units, which correspond to a change in the dye-matrix interaction. The pressure shift allows the determination of the (local) matrix compressibility in an all-optical experiment. The pressure broadening results from the removal of an accidental degeneracy: Different local dye environments, which result in the same shift of the dye transition energy,

respond differently to external pressure.

Since the inhomogeneous broadening of optical lines is a consequence of randomly distributed lattice irregularities in an amorphous solid, it can be described by a statistical theory. The respective model descriptions date back to Markoff[5] and Stoneham[6] and have recently been refined by Laird and Skinner[7] to also include pressure effects on hole spectra. The generality of these theories is restricted by a set of basic assumptions.

Usually it is assumed that one type of interaction (e.g., dispersive forces) between dye and matrix molecules predominates. Also, the matrix units are considered to be spherical and independent of each other, yielding additive contributions to the solvent shift of the embedded dye molecules, which are also assumed to be spherical. Additionally, the matrix units are assumed to be able to arrange themselves independently of each other around a dye molecule.

Laird and Skinner's extension of the statistical approach to describe pressure effects was first applied to dye molecules in various polymer hosts like polyethylene, polystyrene, and polymethylmethacrylate (PMMA). Their prediction of a frequency-dependent pressure shift was duely verified, its predicted magnitude agreeing with the experimental results to within 20%.

The success of this simple approach was surprising, since polymers often meet the above conditions rather poorly. In the case of polymer hosts, the monomer units are taken as the matrix units in the model description. The monomer units clearly are unable to arrange themselves independently, since they are connected by strong directional bonds. Moreover, the monomer units often are slightly polar (as in the case of PMMA).

Furthermore, the range of validity of the results of the statistical model remained unclear, since in the course of the calculation two conflicting limits with regard to the number density ρ of the matrix units within the interaction range of the dye molecule were employed: the high-density limit ($\rho\rightarrow\infty$, the so-called Gaussian approximation) and the low-density limit ($\rho\rightarrow 0$). A consequence of the latter was that correlations between matrix units, arising from their mutual steric exclusion, were neglected.

It was therefore our goal to investigate the statistical description systematically, using model systems that come closest to satisfying the above-mentioned assumptions. For that reason we chose the solid rare gases argon, krypton, and xenon as host matrices. Due to their model character, solid rare gases have been of great interest in the past three decades. Therefore, a large number of data on their properties are readily available (for a review see, e.g., Ref. 8).

In order to avoid the conflicting assumptions with regard to the number density ρ, Sevian and Skinner[9] extended the statistical description by including correlations between the matrix units, arising from their mutual steric exclusion. Retaining the limit of sufficiently large values for ρ, an expression for the inhomogeneous line shape was derived. Furthermore, using Monte Carlo simulations, the authors of Ref. 9 demonstrated that matrix correlations are in fact quantitatively important. A similar statistical model by Messing, Raz, and Jortner[10] also showed better agreement with their spectroscopic data on xenon solvated in liquid argon when the solvent-solvent correlation was taken into account.

The expression for the inhomogeneous line shape derived by Sevian and Skinner[9] allows us to calculate ρ and the depth of the dye-matrix interaction potential from the measured solvent shift and inhomogeneous widths. In order to study the consequences of the conflicting approximations in the original theory (Ref. 7), we evaluate the results at first for the additional limit $\rho\rightarrow 0$.

In order to analyze the effects of external pressure on spectral holes in an analogous way, we extended the statistical description employing Sevian and Skinner's method of including matrix correlations. Furthermore, in our experiments a pressure change is always accompanied by a temperature change, which is due to our sample preparation procedure. Therefore we incorporated the thermal expansion of the matrix, which also contributes to the shift of the transition energies, into the framework of the statistical model. Since the thermal expansion coefficient is known from the literature, the pure pressure effect can be extracted from the measured combined pressure and temperature effects. The local compressibilities in the environment of the dye molecules are calculated with and without the use of the low-density approximation, using different dye-matrix interaction potentials.

II. EXPERIMENT

In order to incorporate free-base phthalocyanine (H_2Pc) into solid rare gases, a cold substrate under vacuum conditions and a suitable furnace are required.[11] The construction of the Knudsen effusion furnace is similar to the one used by Bajema, Gouterman, and Meyer.[12] It consists of a sublimation chamber ($T\approx 600$ K) containing the dye and a superheating chamber ($T\approx 700$ K). Between the chambers, the desired rare gas is added to the vaporized dye. The mixture then enters the superheating chamber and expands through a nozzle into the vacuum surrounding the substrate.

During the sample preparation, the substrate is cooled down to $T\approx 4$ K by a continuous-flow cryostat. After the sample has been deposited, the substrate is immersed into liquid helium. Subsequently, the temperature is lowered to 1.8 K, and a spectral hole is burnt. The helium bath is then sealed off, causing the pressure (and the temperature) to rise. The spectral hole is recorded repeatedly during the pressure increase (for the optical setup see, e.g., Ref. 13). The maximum pressure difference that can be achieved in this way is 0.2 MPa. At the same time the temperature rises to 5 K.

Within our experimental error, the pressure-temperature shift was fully reversible. This is at first surprising, since temperature-cycling experiments on several polymers showed irreversible line shifts.[14] The absence of this effect is probably due to the nanocrystalline nature of thin rare-gas films: Whereas in polymers the TLS allow for structural relaxations of the matrix over a wide time range due to tunneling, in rare-gas films they relax predominatly via thermal activation already at temperatures slightly above 1 K.[15] This gives rise to fast TLS flips well below our experimental time scale.

III. STATISTICAL MODEL

The above-mentioned statistical model description considers an amorphous system of N matrix units, containing a

small concentration of dye molecules. The probability of finding N matrix units at the positions $\vec{R}_1,\ldots,\vec{R}_N$ (the dye molecule is assumed to be located at the coordinate origin) is given by a normalized $(N+1)$-particle distribution function $P(\vec{R}_1,\ldots,\vec{R}_N)$. Each matrix unit will shift the electronic absorption line of the dye molecule by some amount $\tilde{\nu}(\vec{R}_n)$, where $\vec{R}_n$ is the position of the nth matrix unit. If the contributions of all matrix units to the total solvent shift are assumed to be additive, the total inhomogeneous distribution of absorption lines can then be written as[5–7]

$$I(\nu)=\frac{1}{V^N}\int d\vec{R}_1\cdots d\vec{R}_N P(\vec{R}_1,\ldots,\vec{R}_N) \times\delta\left(\nu-\sum_{n=1}^{N}\tilde{\nu}(\vec{R}_n)\right). \tag{1}$$

Replacing the δ function with its Fourier representation and introducing the characteristic function $\Phi(x)$ (Refs. 9, 10, and 16) yields

$$I(\nu)=\frac{1}{2\pi}\int_{-\infty}^{+\infty}dx\ e^{i\nu x}\left\langle\exp\left\{-i\sum_{n=1}^{N}\tilde{\nu}(\vec{R}_n)x\right\}\right\rangle =:\frac{1}{2\pi}\int_{-\infty}^{+\infty}dx\ e^{i\nu x}\Phi(x). \tag{2}$$

The average is defined by

$$\langle\exp\{f(\vec{R}_1,\ldots,\vec{R}_N)\}\rangle =\frac{1}{V^N}\int d\vec{R}_1\cdots d\vec{R}_N P(\vec{R}_1,\ldots,\vec{R}_N) \times\exp\{f(\vec{R}_1,\ldots,\vec{R}_N)\}. \tag{3}$$

In order to avoid the approximation of sufficiently low number densities ρ, which had been applied in an earlier treatment,[7] and to evaluate Eq. (2) in a more general way, Sevian and Skinner performed a cumulant expansion of the characteristic function $\Phi(x)$ up to second-order terms. Since the restriction to these terms will lead to a Gaussian inhomogeneous distribution, as has been shown in Ref. 7, it is referred to as the Gaussian approximation. It is valid in the case of sufficiently large number densities of matrix units within the interaction range of the dye molecule. This approximation is appropriate, since the experimentally measured band shapes are indeed Gaussian.

The next step is the determination of the cumulants (for details see Ref. 9). The first-order cumulant A (the average value) is given by

$$A=\left\langle\sum_{n=1}^{N}\tilde{\nu}(\vec{R}_n)\right\rangle, \tag{4}$$

and the second-order cumulant B (the variance) by

$$B=\left\langle\left(\sum_{n=1}^{N}\tilde{\nu}(\vec{R}_n)\right)^2\right\rangle-\left\langle\sum_{n=1}^{N}\tilde{\nu}(\vec{R}_n)\right\rangle^2. \tag{5}$$

Inserting this result into Eq. (2), we obtain—after carrying out the integration—the following Gaussian inhomogeneous distribution:

$$I(\nu)=\frac{1}{[2\pi\sigma_s^2]^{1/2}}\exp\left[-\frac{(\nu-\nu_s)^2}{2\sigma_s^2}\right], \tag{6}$$

where the solvent shift ν_s of the maximum of the distribution and the full width at half maximum (FWHM) Γ_s are given by

$$\nu_s=A, \tag{7}$$

$$\Gamma_s=2\sqrt{2\ln 2}\sigma_s=2\sqrt{2\ln 2}\times\sqrt{B}.$$

It is interesting to note that in the limit of large number densities $\rho=N/V$ of matrix units the result is always a Gaussian distribution, independent of the specific form of the microscopic solvent-shift function $\tilde{\nu}(\vec{R})$. This is a manifestation of the central limit theorem.[7]

The average values determining the cumulants A and B can now be calculated according to Eq. (3). Using the definition of the two-particle distribution (dye+1 matrix unit) $g(\vec{R}_1)$

$$g(\vec{R}_1)=\frac{1}{V^{N-1}}\int d\vec{R}_2\cdots d\vec{R}_N P(\vec{R}_1,\ldots,\vec{R}_N) \tag{8}$$

the result for the cumulant A is

$$A=\rho\int d\vec{R}\,\tilde{\nu}(\vec{R})g(\vec{R}). \tag{9}$$

An analogous evaluation of the cumulant B using the definition of the three-particle distribution $g_3(\vec{R}_1,\vec{R}_2)$ as

$$g_3(\vec{R}_1,\vec{R}_2)=\frac{1}{V^{N-2}}\int d\vec{R}_3\cdots d\vec{R}_N P(\vec{R}_1,\ldots,\vec{R}_N) \tag{10}$$

yields

$$B=\rho\int d\vec{R}\ g(\vec{R})\tilde{\nu}(\vec{R})^2 +\rho^2\int\int d\vec{R}\,d\vec{R}'V(\vec{R},\vec{R}')\tilde{\nu}(\vec{R})\tilde{\nu}(\vec{R}'). \tag{11}$$

The abbreviation $V(\vec{R},\vec{R}')$ is defined by

$$V(\vec{R},\vec{R}')=g_3(\vec{R},\vec{R}')-g(\vec{R})g(\vec{R}'). \tag{12}$$

At this point, it is interesting to have a closer look at the cumulants A and B. Within the Gaussian approximation, the cumulant B consists of two terms that are proportional to ρ and ρ^2, respectively. In Laird and Skinner's original publication, it was assumed that the number density of matrix units is small enough to allow for the factorization of the $(N+1)$-particle distribution function into a product of two-particle distribution functions

$$P(\vec{R}_1,\ldots,\vec{R}_N)=\prod_{n=1}^{N}g(\vec{R}_n). \tag{13}$$

Inserting the factorization into Eq. (10), we obtain

$$g_3(\vec{R},\vec{R}')=g(\vec{R})g(\vec{R}') \tag{14}$$

and therefore

$$V(\vec{R},\vec{R}')\equiv 0. \tag{15}$$

In this approximation, the terms proportional to ρ^2, which account for the mutual steric exclusion of the matrix units, vanish.

In order to further evaluate the expression for the inhomogeneous distribution [Eq. (6)], the function $\tilde{\nu}(\vec{R})$ describing the perturbations of the transition frequency (the microscopic solvent-shift function) has to be specified. Considering only a nonpolar solute and solvent, $\tilde{\nu}(\vec{R})$ is of the familiar Lennard-Jones type

$$\tilde{\nu}(\vec{R})=\begin{cases} 4\epsilon\left[\left(\dfrac{\sigma}{R-R_0}\right)^{12}-\left(\dfrac{\sigma}{R-R_0}\right)^{6}\right] & \text{if } R\geqslant R_0 \\ \infty \quad \text{if } R<R_0, \end{cases} \tag{16}$$

with the origin shifted by R_0 to account for the large disparity in size between solute and solvent (for details see Ref. 7). In this representation $R_0+\sigma/2$ is the solute radius, whereas $\sqrt[6]{2}\sigma$ can be taken as the solvent diameter. This means that a matrix unit located at the position of the potential minimum $R_0+\sqrt[6]{2}\sigma$ will shift the electronic absorption line of the dye by an amount of the potential depth ϵ as given in Eq. (16).

Furthermore, the dye-matrix distribution function $g(\vec{R})$ and the dye-matrix-matrix distribution function $g_3(\vec{R},\vec{R}')$ have to be specified. For $g(\vec{R})$ a simple step function

$$g(\vec{R})=\begin{cases} 1 \quad \text{if } R\geqslant R_0+R_c \\ 0 \quad \text{if } R<R_0+R_c \end{cases} \tag{17}$$

is chosen, meaning that a matrix unit can be found anywhere with equal probability except within a cavity with radius R_0+R_c containing the dye molecule. The parameter R_c determines how close a matrix unit can approach the dye molecule. With the above conventions about solvent and solute dimensions, we have $R_c=\sigma(1+\sqrt[6]{2})/2\approx 1.061\sigma$.

Applying the Kirkwood superposition approximation,[9,10,16] $g_3(\vec{R},\vec{R}')$ is factorized as

$$g_3(\vec{R},\vec{R}')\approx g(\vec{R})g(\vec{R}')g_s(|\vec{R}-\vec{R}'|), \tag{18}$$

introducing a matrix-matrix distribution $g_s(|\vec{R}-\vec{R}'|)$. In analogy to the dye-matrix distribution, we insert a simple step function for $g_s(|\vec{R}-\vec{R}'|)$

$$g_s(|\vec{R}-\vec{R}'|)=\begin{cases} 1 \quad \text{if } |\vec{R}-\vec{R}'|\geqslant R_s \\ 0 \quad \text{if } |\vec{R}-\vec{R}'|<R_s, \end{cases} \tag{19}$$

excluding the volume of a matrix unit (diameter $\sqrt[6]{2}\sigma$) as a possible location for other matrix units. A numerical evaluation of the cumulants A and B (with and without matrix correlations) yields the number density ρ and the depth of the dye-matrix interaction potential ϵ from the measured solvent shift and inhomogeneous widths (see Sec. IV).

The simple step functions as given in Eqs. (17) and (19) are a very crude approximation for the radial distribution functions in condensed matter. In a van der Waals fluid consisting of identical spherical particles, for instance, the distribution function starts out with a value distinctly larger than 1 and exhibits an oscillatory behavior corresponding to the solvent shell structure. Only at distances of several solvent shells, it approaches the limiting value of 1.[17] We do not use such more realistic distributions in our calculations since we have no information on their detailed forms for the rare-gas systems. According to the discussion in Sec. IV, there are indications that the dopant molecules are located between the crystalline grains of the rare-gas films in regions of rather low local density. Details of the form of the radial distributions would be quite speculative in these regions. We wish to mention, however, that in the case of polymeric samples more complicated distribution functions were used in the interpretation of inhomogeneous line parameters and of pressure effects on hole spectra and better agreement between theory and experiment was obtained as compared to the simple step functions.[18] For polymeric dye-matrix systems, additional experimental data are available, namely, the pressure broadening of the hole spectra (because the experiments can be performed in a closed pressure cell at constant temperature) and the variation of the pressure shift parameter with the optical frequency (due to the broader inhomogeneous bands).

Let us now turn to the question of pressure effects on spectral holes. As mentioned above, in our experiments the pressure change is accompanied by a simultaneous change in temperature. Therefore, the observed hole shifts and broadenings will not only be due to pressure changes, but also to the thermal expansion of the matrix. In addition, there may also be dynamical effects such as phonon scattering and (fast) TLS relaxations, which we will not treat in this contribution.

Pure pressure effects have been accounted for by the Laird and Skinner theory[7] (in the low-density limit). This theory can be conveniently expanded to also include the thermal expansion of the matrix and its influence on the dye molecule. Furthermore, we will also take into account, as in the case of the inhomogeneous distribution, the mutual steric exclusion of matrix units, which is not treated in Ref. 7.

In analogy to the inhomogeneous distribution [Eq. (1)], the pressure-temperature kernel $f(\nu'|\nu,\Delta p,\Delta T)$, i.e., the probability that a guest molecule with the original solvent shift ν will have a new transition frequency ν' after a pressure change Δp and a temperature change ΔT, can be written as

$$f(\nu'|\nu,\Delta p,\Delta T)=\frac{1}{I(\nu)V^N}\int d\vec{R}_1\cdots d\vec{R}_N P(\vec{R}_1,\ldots,\vec{R}_N)\,\delta\left(\nu-\sum_{n=1}^{N}\tilde{\nu}(\vec{R}_n)\right)\delta\left(\nu'-\sum_{n=1}^{N}\tilde{\nu}'(\vec{R}_n;\Delta p;\Delta T)\right). \tag{20}$$

Starting out with a distribution of absorbers $i(\nu)$, e.g., a spectral hole, the new distribution of $i(\nu')$ after the temperature and pressure change will then be given by

$$i(\nu';\Delta p;\Delta T)=\int_{-\infty}^{+\infty} d\nu\; f(\nu'|\nu,\Delta p,\Delta T)i(\nu). \quad (21)$$

The experimentally observed pressure-temperature shift was always found to be linear (see Fig. 3, squares), while the concomitant hole broadening can be described by a power law. The latter is clearly dominated by dynamical processes that are affected by the temperature change. For polymeric samples, the pure pressure shift was also shown to be linear, and the pure pressure broadening was proportional to the absolute magnitude of the pressure change.[13] The same behavior is now assumed to be valid for the effects of the pure thermal volume expansion. The function $\tilde{\nu}'(\vec{R}_n;\Delta p;\Delta T)$ in Eq. (20) can then be linearized to

$$\tilde{\nu}'(\vec{R}_n;\Delta p;\Delta T)=\tilde{\nu}(\vec{R}_n)+\tilde{\alpha}(\vec{R}_n)\Delta p+\tilde{\beta}(\vec{R}_n)\Delta T, \quad (22)$$

with

$$\tilde{\alpha}(\vec{R}):=-\frac{\partial\tilde{\nu}(\vec{R})}{\partial R}\,\kappa\,\frac{R}{3}; \quad \tilde{\beta}(\vec{R}):=\frac{\partial\tilde{\nu}(\vec{R})}{\partial R}\,\gamma\,\frac{R}{3}. \quad (23)$$

κ is the compressibility and γ the volume thermal expansion coefficient of the matrix. It is important to note that the temperature and pressure effects have opposite signs [see Eq. (23) and Refs. 13, 19].

Using again the Fourier representations for the δ functions in Eq. (20), we obtain for the characteristic function

$$\Psi(x,y)=\left\langle \exp\left\{ -i\sum_{n=1}^{N}\left[\tilde{\nu}(\vec{R}_n)x+\tilde{\alpha}(\vec{R}_n)\Delta p y+\tilde{\beta}(\vec{R}_n)\Delta T y\right]\right\}\right\rangle. \quad (24)$$

Performing a cumulant expansion of Eq. (24) and applying the Gaussian approximation, we arrive after a subsequent Taylor expansion at

$$\ln\Psi(x,y)\approx -iAx-iA'\Delta p y-iA''\Delta T y-\tfrac{1}{2}Bx^2-\tfrac{1}{2}B'\Delta p^2y^2-\tfrac{1}{2}B''\Delta T^2y^2-C\Delta p y x-D\Delta T y x-E\Delta p\Delta T y^2. \quad (25)$$

The cumulants A', A'', B', B'', C, D, and E, are evaluated according to the procedure described by Sevian and Skinner[9] for the case of the inhomogeneous distribution. The results are given in the Appendix.

Substituting this result into Eq. (20), one obtains a Gaussian conditional probability

$$f(\nu'|\nu,\Delta p,\Delta T)=\frac{1}{\sqrt{2\pi[\Delta\sigma(\Delta p,\Delta T)]^2}}\times\exp\left[-\frac{[\nu'-\nu-\Delta\nu(\nu,\Delta p,\Delta T)]^2}{2[\Delta\sigma(\Delta p,\Delta T)]^2}\right]. \quad (26)$$

The pressure-temperature shift is given by

$$\Delta\nu(\nu,\Delta p,\Delta T)=\left[A'+\frac{C(\nu-A)}{B}\right]\Delta p+\left[A''+\frac{D(\nu-A)}{B}\right]\Delta T. \quad (27)$$

Pressure and temperature contributions to the total line shift are additive and linear in Δp and ΔT, respectively. The magnitude of the pressure-temperature shift depends on the optical frequency ν, which is not the case for the pressure-temperature broadening

$$\Delta\sigma(\Delta p,\Delta T)=\left[\left(B'-\frac{C^2}{B}\right)(\Delta p)^2+\left(B''-\frac{D^2}{B}\right)(\Delta T)^2+2\left(E-\frac{CD}{B}\right)(\Delta p\Delta T)\right]^{1/2}. \quad (28)$$

It can be shown that

$$\Delta\sigma(\Delta p,\Delta T)\propto|\gamma\Delta T-\kappa\Delta p|. \quad (29)$$

This equation predicts that for certain pressure and temperature changes, the pressure and temperature contributions should compensate each other. This effect, however, cannot be observed experimentally for the rare-gas systems, since the hole broadening is dominated by dynamical scattering processes. The dependence of the pure pressure broadening (i.e., for $\Delta T=0$) on the absolute magnitude of the pressure change has been verified for polymeric systems.[13]

The next step is the evaluation of the cumulants using the step functions (17) and (19). In order to simplify the calculations, we consider at first a purely attractive van der Waals potential $\tilde{\nu}(\vec{R})\propto -1/R^6$. This approximation seems reasonable, since only matrix units located in the attractive part of the intermolecular potential can cause the observed redshift in pure pressure-tuning experiments.[13] We obtain the following simple relations for the cumulants

$$A'=2\kappa A; \quad A''=-2\gamma A; \quad C=2\kappa B; \quad D=-2\gamma B;$$
$$B'=4\kappa^2B; \quad B''=4\gamma^2B; \quad E=-4\kappa\gamma B. \quad (30)$$

Inserting these results into Eq. (28) yields for the pressure-temperature broadening

$$\Delta\sigma(\Delta p,\Delta T)=0. \quad (31)$$

For the pressure-temperature shift [Eq. (27)], we obtain

$$\Delta\nu(\nu,\Delta p,\Delta T)=2[\kappa\Delta p-\gamma\Delta T]\nu. \quad (32)$$

It is interesting to note that expression (32) holds true also in the absence of matrix correlations, since all cumulants containing higher-order terms cancel out when inserted into Eq. (27). ν is the burning frequency of the spectral hole in the inhomogeneous band with respect to the gas-phase position of dye transition frequency. For evaluating Eq. (32), we have to take into account that the volume thermal expansion coefficient γ depends, in contrast to the compressibility, strongly on the temperature, even in the small temperature interval between 1.8 and 5 K. Fortunately, experimental data for $\gamma(T)$ are available for crystalline solid rare-gas samples.[20]

Therefore we can substitute $\gamma\Delta T \rightarrow \int_{T_0}^{T_0+\Delta T} \gamma(T)dT$ in Eq. (32), where T_0 is the burning temperature of the hole.

With the modified Eq. (32), we have an analytical expression for extracting the pure pressure shift from our pressure-temperature data. In order to test the reliability of this procedure, we reevaluated data measured in the same fashion in a H_2Pc-doped partially crystalline polyethylene sample.[14] With the known pure pressure shift[13] and thermal expansion coefficient,[21] we obtained agreement with the experimental data within 20%. We can take this figure as an upper bound for the error of our calculations.

Equation (32) also predicts that the static pressure and temperature shifts should compensate each other for a certain choice of Δp_{comp} and ΔT_{comp} values. Setting $\Delta\nu(\nu,\Delta p,\Delta T)=0$ one obtains the relation

$$\Delta p_{\text{comp}} = \frac{1}{\kappa} \int_{T_0}^{T_0+\Delta T_{\text{comp}}} \gamma(T)dT. \tag{33}$$

Inserting for a typical experimental situation $T_0=1.8$ K and $\Delta T_{\text{comp}}=3.1$ K as well as using the crystal literature data at $T=4$ K for the compressibility $\kappa_{\text{lit}}=0.375$ GPa^{-1} (for argon) (Ref. 22) and the temperature-dependent data for the volume thermal expansion coefficient $\gamma(T)$,[20] yields $\Delta p_{\text{comp}}=0.0461$ MPa. Δp and ΔT, however, are not independent in our case, but are connected by the vapor pressure diagram. According to the latter, the temperature increase of $\Delta T=3.1$ K corresponds to a pressure increase of $\Delta p=0.2$ MPa. The fact that the actual pressure increase is larger than the value Δp_{comp}, for which temperature and pressure shifts should compensate each other, means that in general the line-shift behavior is dominated by pressure effects. This result, which also holds for krypton and xenon, is confirmed by the observed redshift as was found in pure pressure-tuning experiments on polymers.[13]

Equation (32) has been used numerous times to determine the compressibility in pure pressure experiments (i.e., in the case of $\Delta T=0$). Contrary to Eq. (31), however, a nonzero pressure broadening was observed. In order to obtain a nonvanishing pressure broadening, the Lennard-Jones potential [Eq. (16)], which contains a repulsive term, has to be used instead of the simple van der Waals potential. In this case the cumulants in Eq. (27) have to be evaluated numerically. In order to account for the temperature dependence of the thermal expansion, the volume thermal expansion coefficient γ in the cumulants A'', B'', D, and E must be replaced by its average

$$\gamma \rightarrow \bar{\gamma} = \frac{1}{\Delta T} \int_{T_0}^{T_0+\Delta T} \gamma(T)dT, \tag{34}$$

which leads to a temperature dependence of these particular cumulants.

In the following, we will restrict our considerations to the evaluation of the line shift.

IV. RESULTS AND DISCUSSION

Figure 1 shows a broadband absorption spectrum of H_2Pc in argon recorded at a temperature of 4 K. The spectrum is dominated by two absorption bands. Following Bajema, Gouterman, and Meyer,[12] the lower-energy component is labeled the Q_x band, the higher-energy one the Q_y band. Both of these bands correspond to the electronic $S_0 \rightarrow S_1$ transition, which is degenerate in metal phthalocyanines. When the central metal atom is replaced by two hydrogen atoms, the D_{4h} symmetry is reduced to D_{2h}. This lifts the degeneracy of the Q band, leading to the observed Q_x and Q_y peaks.[23] A number of vibronic 0-1 transitions are also visible, whose transition energies agree with the strongest lines of the H_2Pc excitation spectrum measured by Bondybey and English.[24] The spectral positions and inhomogeneous widths of the Q_x bands in argon, krypton, and xenon are listed in Table I. An increasing redshift of the inhomogeneous bands with respect to the H_2Pc gas-phase absorption frequency of 15 128 cm^{-1} (Ref. 23) from argon to xenon is observed, which is a consequence of the increasing matrix polarizability. At the same time the inhomogeneous widths also increase, which can be explained by purely statistical considerations (see, e.g., Ref. 11). Table I also lists the Lennard-Jones parameter σ for the rare gases investigated (see, e.g., Ref. 25 and references therein) as well as the potential shift R_0, which was calculated using the known H_2Pc radius of 6.5 Å.[26] R_0 decreases from argon to xenon, since the correction was chosen such that the limit $R_0 \rightarrow 0$ describes dye and matrix molecules of equal size.

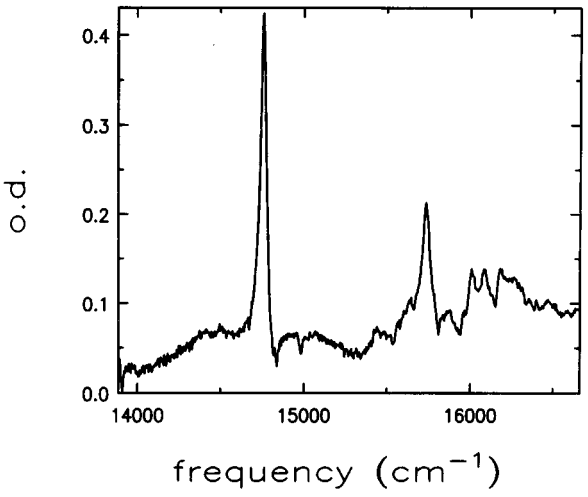

FIG. 1. Broadband absorption spectrum of H_2Pc in argon at $T=4$ K. The optical density is plotted vs the frequency in units of wave numbers.

In order to investigate the influence of matrix correlations, which were neglected in Laird and Skinner's original model,[7] we now determine the potential parameter ϵ and the

TABLE I. Measured solvent shift ν_s and inhomogeneous width Γ_s (FWHM) of the Q_x band of H_2Pc. Also listed are the radial potential shift R_0 and the Lennard-Jones parameter σ of the matrix (Ref. 25).

	ν_s (cm^{-1})	Γ_s (cm^{-1})	R_0 (Å)	σ (Å)
Argon	−364	44	4.798	3.405
Krypton	−464	58	4.68	3.65
Xenon	−593	89	4.51	3.98

TABLE II. Comparison of calculated potential depths and number densities of matrix units with ($\epsilon_{\rm corr}$, $\rho_{\rm corr}$) and without (ϵ,ρ) matrix correlations. $\rho_{\rm cryst}$ are the crystalline number densities (Refs. 22, 28, 29).

	ϵ ($\rm cm^{-1}$)	$\epsilon_{\rm corr}$ ($\rm cm^{-1}$)	ρ ($\rm Å^{-3}$)	$\rho_{\rm corr}$ ($\rm Å^{-3}$)	$\rho_{\rm cryst}$ ($\rm Å^{-3}$)
Argon	1.57	23.1	0.145	0.00975	0.0267
Krypton	2.45	33.4	0.104	0.00787	0.0222
Xenon	4.58	47.5	0.062	0.00594	0.0173

number density ρ of matrix units within the interaction range of the dye molecule from the measured solvent-shift values and inhomogeneous widths using the relations (7). As mentioned above, the cumulants A and B are evaluated numerically for both cases. For the case of vanishing correlations $[V(\vec{R},\vec{R}')\equiv 0]$, an analytical evaluation of the cumulants is possible,[27] yielding identical results.

The results are summarized in Table II. Let us look first at the case of vanishing matrix correlations. The first column shows the potential parameter ϵ. As expected, the model yields an increasing depth of the interaction potential from argon to xenon reflecting the increasing matrix polarizability. Also, the number density ρ (third column) shows the expected behavior, namely, a decrease from argon to xenon due to the increase in size of the matrix units. Both parameters therefore exhibit a qualitatively correct behavior. A closer inspection of the magnitude of these values, however, is necessary.

The last column of Table II lists the number densities $\rho_{\rm cryst}$ (Refs. 22, 28, 29) in bulk rare-gas crystals at $T=4$ K. Since the considered rare gases form face-centered cubic (fcc) structures (which have the highest possible packing fraction), these values define an upper bound of possible number densities. In all three cases, our calculation yields unrealistic results, where the values for ρ exceed $\rho_{\rm cryst}$ by far, which means that the model calculation is based on too many matrix units.

In this light, the results for ϵ also require closer scrutiny. Since all the parameters determining the perturbation of the transition frequency [Eq. (16)] are now known, we can test the ϵ values by modeling a solvent-shell structure around the cavity containing the dye molecule and then calculating the resulting solvent-shift using Eq. (16). We now choose spherical equidistant ($\Delta R=\sqrt[6]{2}\sigma$) solvent shells with the first shell at the equilibrium distance $R_0+\sqrt[6]{2}\sigma$ (for details see Ref. 30). No interstitial positions between the individual shells are allowed. One obtains for the total solvent shift of M solvent shells

$$\nu_s(M)=\sum_{n=1}^{M}\tilde{\nu}(R_0+n\sqrt[6]{2}\sigma)\,\frac{4\pi(R_0+n\sqrt[6]{2}\sigma)^2}{(\sqrt[6]{2}\sigma)^2}, \quad (35)$$

where $\tilde{\nu}(R_0+n\sqrt[6]{2}\sigma)$ is the value of the perturbation function of the transition frequency (16) for the nth solvent shell. This particular arrangement of matrix units corresponds to a packing fraction of roughly 52%. This fairly small packing fraction was chosen to account for the nanocrystalline structure of the rare-gas films.[15] Evaluating Eq. (35) for $M\to\infty$, one obtains only 29% of the observed solvent shift in the case of argon, 33% for krypton, and 43% for xenon. Obviously each matrix unit would have to contribute much more strongly to the solvent shift in order to reproduce the experimental findings. This result highlights the problems of the factorization of $P(\vec{R}_1,\ldots,\vec{R}_N)$ [Eq. (13)]: By neglecting correlations between the matrix units, more than one molecule can occupy the same position. This reinforces the notion that the theoretical treatment is therefore based on too many matrix units, giving insufficient weight to the individual solvent molecule. This interpretation is in agreement with the fact that the calculated number densities ρ (see above) are far too large. Even if the crystalline packing fraction (that is, crystalline number densities $\rho_{\rm cryst}$) were chosen, it would still be impossible to reproduce the measured solvent shift.

Therefore the necessity to abandon the factorization (13), which is reasonable only in the low-density limit, and to include the mutual steric exclusion of the matrix units becomes clear. We now recalculate the potential parameter and the number density. The results $\epsilon_{\rm corr}$ and $\rho_{\rm corr}$ with matrix correlations taken into account are also given in Table II.

For all matrices, the potential parameter $\epsilon_{\rm corr}$ is now significantly larger, whereas the number density $\rho_{\rm corr}$ is reduced approximately by the same factor. The problem of unrealistically large number densities is eliminated. In fact, in the case of argon, $\rho_{\rm corr}$ corresponds to a packing fraction of only 28%, which compares to a value of 74% for the crystalline fcc structure. When condensed at low temperatures, rare-gas films exhibit a nanocrystalline structure with grain sizes as small as 10 nm.[31] A simple estimate provides an idea of the density in the regions between the crystallites. It is known from the literature that the total density of an argon film condensed at $T=4$ K is smaller than that of the bulk material by about 35%.[31] Assuming that half of the atoms are contained in the crystallites,[32] we estimate the density in the interstitial regions as $\rho_{\rm int}\approx 0.012$ $\rm Å^{-3}$. Considering the crudeness of this procedure, this value is surprisingly close to our value for $\rho_{\rm corr}$. This lends weight to the expectation that the large dye molecules are located between the grains of the rare-gas matrices.

In spite of the low number density, the observed solvent shift can now be accounted for due to the significantly larger potential parameter $\epsilon_{\rm corr}$ for a large variety of matrix unit arrangements that are consistent with the low number density. Hence, it turns out that the introduction of matrix correlations is crucial for obtaining realistic values for the potential parameter and the number density and is able to resolve the problems encountered with the simpler model.

The fact that only few matrix atoms are needed to produce the observed bulk solvent shift has been demonstrated in jet-expanded molecular beams of dye-$(\rm RG)_n$ heteroclusters, where RG stands for the rare gases argon, krypton, and xenon. For a variety of dye molecules, the groups of Jortner and Even,[33-36] as well as Leutwyler and Bösiger[37] measured the solvent shift as a function of the number n of matrix atoms contained in the clusters. In the dichloroanthracene-argon heterocluster,[36] for example, it was found that the first 34 argon atoms generate already 81% of the total bulk solvent shift.

Furthermore, since the potential depth ϵ in our model describes the shift of the electronic absorption line of the dye molecule due to a matrix unit located at the position of the

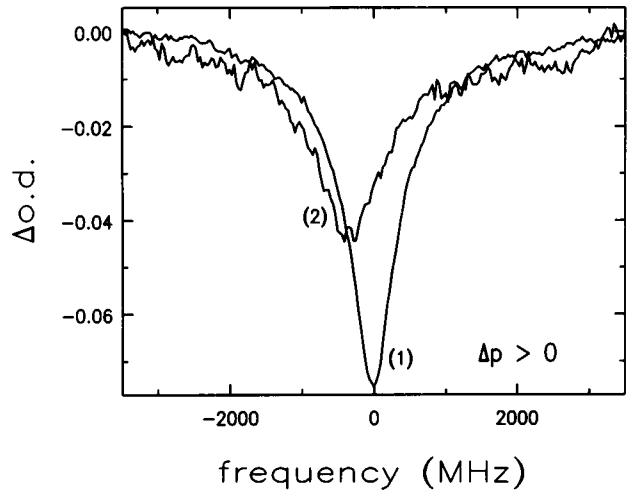

FIG. 2. Pressure shift and broadening of a spectral hole (H_2Pc in argon). Trace (1): Original hole profile; trace (2): spectral hole after a pressure increase of 88 kPa.

potential minimum $R_0+\sqrt[6]{2}\sigma$ [see Eq. (16)], its value should be comparable to the solvent shift in a dye-Ar_1 heterocluster. Unfortunately, no experiments have been performed using H_2Pc. Still, for the dye molecules investigated in Refs. 33–37, the solvent shift caused by the first argon atom in a heterocluster amounted to between 6% and 8% of the bulk solvent shift. In our case, the ratio $\epsilon_{\mathrm{corr}}/\nu_s$ also falls within this range. This provides a rough confirmation of the magnitude of our calculated potential depths ϵ_{corr}.

Let us now turn to the pressure-tuning experiments. Figure 2 shows the pressure shift and broadening of a spectral hole (H_2Pc in argon). Trace (1) shows the spectral hole, while trace (2) displays the hole profile after a pressure increase of 88 kPa. Even this small pressure change produces detectable changes in the hole profile.

In Fig. 3 the shift of the hole center $\Delta\nu$ is plotted versus the pressure change Δp. As mentioned above, the pressure change is accompanied by a simultaneous change in temperature. The squares denote the raw data including the temperature effects. In order to investigate the effects of the different potentials and of neglected matrix correlations, we evaluate these data in several ways to determine the matrix compressibility.

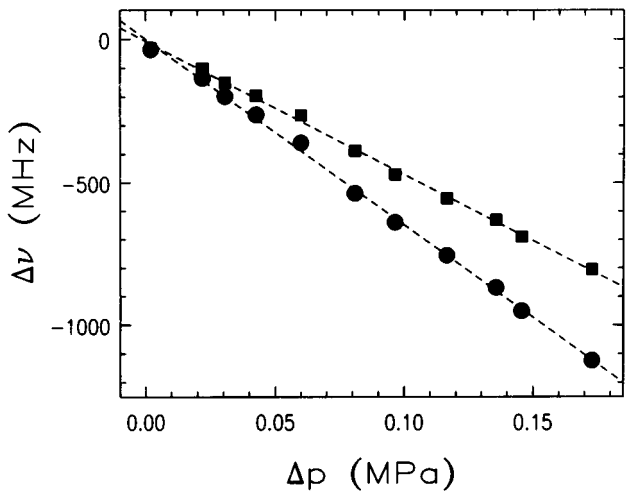

FIG. 3. Shift of hole center vs pressure change (H_2Pc in argon): Raw data without correction (squares) and data after temperature correction (circles). For details see text.

TABLE III. Numerically determined matrix compressibilities $\kappa_{\mathrm{LJ,corr}}$ (with correlations) and κ_{LJ} (without correlations) using the Lennard-Jones potential as well as analytically calculated compressibilities κ_{vdW} for the van der Waals potential. κ_{Lit} are literature data for bulk crystals (Ref. 39).

	κ_{vdW} (GPa^{-1})	κ_{LJ} (GPa^{-1})	$\kappa_{\mathrm{LJ,\,corr}}$ (GPa^{-1})	κ_{Lit} (GPa^{-1})
Argon	0.276	0.260	0.265	0.350
Krypton	0.290	0.276	0.280	0.299
Xenon	0.419	0.399	0.389	0.274

(i) For the case of the purely attractive van der Waals potential the matrix compressibility κ_{vdW} is calculated using the modified Eq. (32), inserting literature data for $\gamma(T)$.[20] As pointed out above, Eq. (32) is valid with and without matrix correlations taken into account. The results are given in Table III.

(ii) For the Lennard-Jones potential [Eq. (16)] the cumulants in Eq. (27) have to be evaluated numerically. To simplify the calculation, we evaluate the pressure and temperature contributions in Eq. (27) separately. In a first step the contribution to the measured total shift (see Fig. 3, squares) of the spectral hole caused by the thermal expansion is calculated numerically for each data point according to

$$\Delta\nu(\nu,\Delta p=0,\Delta T)=\left[A''(T_0,\Delta T)+\frac{D(T_0,\Delta T)}{B}\,(\nu-A)\right]\Delta T \tag{36}$$

and subtracted from the measured total shift to yield the pure pressure shift. The cumulants in Eq. (36) are calculated for both cases, with and without matrix correlations. The resulting pure pressure shift for the former case is shown in Fig. 3 (circles). Due to the opposite sign of pressure and temperature shifts [Eqs. (23)], the pure pressure shifts is larger than the measured total shift. In the second step, the pure pressure shift is analyzed numerically [using Eq. (27) with $\Delta T=0$] to determine the compressibilities κ_{LJ} without matrix correlations and $\kappa_{\mathrm{LJ,\,corr}}$ including matrix correlations (see Table III).

It can be seen that within the error limits mentioned above, the value for the compressibility does not change when matrix correlations are taken into account. Even the restriction to the simple van der Waals potential does not change the calculated compressibilities to a large extent. These results point to a loose packing of the matrix units around the dye molecules, since they seem to be located in that part of the potential that can be approximated by an R^{-6} power law. From these results we conclude that for the optical determination of the matrix compressibility the simple approach using the van der Waals potential and neglecting matrix correlations is sufficient, justifying previous compressibility determinations in a variety of samples according to Eq. (32).

The same behavior was also observed in the polymeric hosts polyethylene and polymethylmethacrylate, doped with H_2Pc.[38] Whereas the compressibility remained unchanged, ρ and ϵ also had to be adjusted significantly when matrix correlations were introduced. In these polymers the optically determined compressibilities agree quite well with the mechanically measured values. This does not seem to be the case for rare-gas matrices (except for krypton), as can be seen from a comparison with the literature values $\kappa_{\mathrm{Lit}}(T=4$ K) (Ref. 39) (see Table III). The compressibilities κ_{Lit}, however, were measured in bulk rare-gas crystals. For the nanocrystalline rare-gas films used in our experiments, no compressibility measurements have been reported so far. One would expect, however, that the compressibility of these films is larger than in crystalline samples due to a more open structure with many voids. This is indeed the case for xenon. In this light the rather low compressibility value that we obtained for argon films is puzzling. One has to keep in mind, however, that the compressibilities accessible through hole-burning experiments reflect the properties of the local environment of the dye molecule. The large number of randomly oriented, interlocking grains could produce a shielding effect, which means that the effective pressure at the site of the guest molecule is smaller than the value applied (and measured) externally. This would reduce the calculated compressibility and would project the picture of a seemingly ''harder'' environment. Depending on the actual structure of the films, these two effects will combine to various degrees. At the present stage, however, no definite interpretation is possible.

It was shown in Ref. 40 that the sizes of the crystallites depend strongly on the condensation temperature of the samples. For a fixed condensation temperature, as was the case in our experiments, different rare gases will exhibit a different density deficit with respect to the density in the crystal. Since the difference between condensation temperature and sublimation temperature was largest in xenon, its film density deviated most from the crystalline density. Therefore it is difficult to compare the different rare-gas matrices, since they are in different structural states. This also makes the comparison with crystalline data problematic.

To clarify these points, further experiments are needed. It has already been shown that annealing changes the structure of the films significantly as grain sizes tend to increase.[41] The effects of these changes on the compressibility and on the number density should provide valuable information about the local environment of the dye molecule.

In principle, Eq. (28) can be used to investigate the role of matrix correlations for the pressure-broadening effects. However, as mentioned above, the hole width after a temperature change is not only influenced by the thermal expansion, which is accounted for in Eq. (28), but also by temperature-dependent dynamical processes such as scattering of local modes and TLS. The latter contribution cannot be measured separately for the rare-gas systems. One can, however, evaluate Eq. (28) numerically for the Lennard-Jones potential to predict the contribution of pressure and thermal expansion to the total broadening, since all required parameters have been determined from the available experimental data. It turns out that this contribution is negligible.[42] Hence, the observed hole broadening after a pressure-temperature change is dominated by the dynamical processes.

V. SUMMARY

In this paper we presented an extension of a widely applied statistical theory to describe the inhomogeneous broadening of spectral lines as well as pressure effects on hole-burning spectra. In its original form this model was remarkably successful in determining the compressibility of polymer matrices from the measured spectral shift of persistent hole spectra. The basic assumptions of the model, however, are satisfied only to a limited extent in polymeric hosts. In addition, two conflicting approximations with respect to the number density of the matrix units were made. We therefore decided to investigate the statistical description systematically and to test the consequences of the approximations made in the original model by applying it to systems that come closest to satisfying the basic assumptions. This is the case for dye-doped solid rare-gas matrices. In order to make pressure-tuning experiments possible, we built a novel cryostat that allowed us to immerse the sample into liquid helium after its condensation onto a cold substrate.

Measured quantities were the solvent shift and the width of the inhomogeneously broadened Q_x absorption band as well as the pressure shift of the spectral holes. From these data, the depth of the dye-matrix interaction potential, the number density of matrix units within the interaction range of the dye molecule, and the matrix compressibility were calculated. Analyzing the data using the original model leads to unrealistic values for potential parameters and number densities. For this reason an existing modification of the statistical theory, which takes into account correlations between matrix units due to their mutual steric exclusion, was further extended to also describe pressure effects on spectral holes. Furthermore, the hole shifts due to the thermal expansion of the matrix were incorporated into the statistical description, since in our experiments a pressure change was inevitably accompanied by a change of the temperature. A new analysis of our experimental data with the expanded model now yields physically reasonable potential parameters and number densities. A further interesting result is the fact that the optically determined compressibilities do not change upon inclusion of the matrix correlations. Moreover, the compressibilities remain unchanged when a purely attractive van der Waals dye-matrix interaction potential is used instead of the more complicated Lennard-Jones-type potential. This means that for an optical determination of the matrix compressibilities the simple analytical equation based on a purely attractive van der Waals potential is a rather good approximation. This result justifies earlier compressibility determinations using the simple model.

ACKNOWLEDGMENTS

We would like to thank W. Richter and Th. Giering for valuable discussions as well as the ''Deutsche Forschungsgemeinschaft'' and the ''Fonds der Chemischen Industrie'' for financial support.

APPENDIX

$$A' = \rho \int d\vec{R} g(\vec{R}) \tilde{\alpha}(\vec{R}), \tag{A1}$$

$$A'' = \rho \int d\vec{R} g(\vec{R}) \tilde{\beta}(\vec{R}), \tag{A2}$$

$$B' = \rho \int d\vec{R} g(\vec{R}) \tilde{\alpha}(\vec{R})^2 + \rho^2 \int\int d\vec{R} d\vec{R}' V(\vec{R},\vec{R}') \tilde{\alpha}(\vec{R}) \tilde{\alpha}(\vec{R}'), \tag{A3}$$

$$B'' = \rho \int d\vec{R} g(\vec{R}) \tilde{\beta}(\vec{R})^2 + \rho^2 \int\int d\vec{R} d\vec{R}' V(\vec{R},\vec{R}') \tilde{\beta}(\vec{R}) \tilde{\beta}(\vec{R}'), \tag{A4}$$

$$C = \rho \int d\vec{R} g(\vec{R}) \tilde{\nu}(\vec{R}) \tilde{\alpha}(\vec{R}) + \rho^2 \int\int d\vec{R} d\vec{R}' V(\vec{R},\vec{R}') \tilde{\nu}(\vec{R}) \tilde{\alpha}(\vec{R}'), \tag{A5}$$

$$D = \rho \int d\vec{R} g(\vec{R}) \tilde{\nu}(\vec{R}) \tilde{\beta}(\vec{R}) + \rho^2 \int\int d\vec{R} d\vec{R}' V(\vec{R},\vec{R}') \tilde{\nu}(\vec{R}) \tilde{\beta}(\vec{R}'), \tag{A6}$$

$$E = \rho \int d\vec{R} g(\vec{R}) \tilde{\alpha}(\vec{R}) \tilde{\beta}(\vec{R}) + \rho^2 \int\int d\vec{R} d\vec{R}' V(\vec{R},\vec{R}') \tilde{\alpha}(\vec{R}) \tilde{\beta}(\vec{R}'), \tag{A7}$$

The function $V(\vec{R},\vec{R}')$ is defined as

$$V(\vec{R},\vec{R}') = g_3(\vec{R},\vec{R}') - g(\vec{R}) g(\vec{R}'). \tag{A8}$$

*Present address: Department of Chemistry, University of California, Riverside, CA 92512.

[1] B. M. Kharlamov, R. I. Personov, and L. A. Bykovskaja, Opt. Commun. **12**, 191 (1974).
[2] A. A. Gorokhovskiĭ, R. K. Kaarli, and L. A. Rebane, Pis'ma Zh. Eksp. Teor. Fiz. **20**, 474 (1974) [JETP Lett. **20**, 216 (1974)].
[3] J. Friedrich and D. Haarer, Angew. Chem. **96**, 96 (1984); Angew. Chem. Int. Ed. Engl. **23**, 113 (1984).
[4] K. A. Littau, Y. S. Bai, and M. D. Fayer, J. Chem. Phys. **92**, 4145 (1990).
[5] A. A. Markoff, *Wahrscheinlichkeitsrechnung* (Teubner, Leipzig, 1912).
[6] A. M. Stoneham, Rev. Mod. Phys. **41**, 82 (1969).
[7] B. B. Laird and J. L. Skinner, J. Chem. Phys. **90**, 3274 (1989).
[8] G. L. Pollak, Rev. Mod. Phys. **36**, 748 (1964).
[9] H. M. Sevian and J. L. Skinner, Theor. Chim. Acta **82**, 29 (1992).
[10] I. Messing, B. Raz, and J. Jortner, J. Chem. Phys. **66**, 2239 (1977).
[11] P. Geissinger and D. Haarer, Chem. Phys. Lett. **197**, 175 (1992).
[12] L. Bajema, M. Gouterman, and B. Meyer, J. Mol. Spectrosc. **27**, 225 (1968).
[13] Th. Sesselmann, W. Richter, D. Haarer, and H. Morawitz, Phys. Rev. B **36**, 7601 (1987).
[14] L. Kador, Diploma thesis, University of Bayreuth, 1984.
[15] L. Hornig, B. Döttling, G. Weiss, S. Hunklinger, and F. Baumann, Z. Phys. B **86**, 217 (1992).
[16] S. H. Simon, V. Dobrosavljević, and R. M. Stratt, J. Chem. Phys. **93**, 2640 (1990).
[17] Y. Tang and B.C.-Y. Lu, J. Chem. Phys. **100**, 3079 (1994).
[18] L. Kador, P. Geissinger, and D. Haarer, J. Lumin. **64**, 101 (1995).
[19] M. N. Sapozhnikov, J. Chem. Phys. **68**, 2352 (1978).
[20] C. R. Tilford and C. A. Swenson, Phys. Rev. B **5**, 719 (1972).
[21] G. K. White and C. L. Choy, J. Polym. Sci. Polym. Phys. Ed. **22**, 835 (1984).
[22] O. G. Peterson, D. N. Batchfelder, and R. O. Simmons, Phys. Rev. **150**, 703 (1966).
[23] P. S. H. Fitch, L. Wharton, and D. H. Levy, J. Chem. Phys. **73**, 1064 (1980).
[24] V. E. Bondybey and J. H. English, J. Am. Chem. Soc. **101**, 3446 (1979).
[25] *Rare Gas Solids*, edited by M. L. Klein and J. A. Venables (Academic, London, 1977).
[26] I. Chen, J. Mol. Spectrosc. **23**, 131 (1967).
[27] L. Kador, J. Chem. Phys. **95**, 5574 (1991).
[28] D. R. Sears and H. P. Klug, J. Chem. Phys. **37**, 3002 (1962).
[29] D. L. Losee and R. O. Simmons, Phys. Rev. **172**, 944 (1968).
[30] P. Geissinger, W. Richter, and D. Haarer, J. Lumin. **56**, 109 (1993).
[31] L. Hornig, N. Schnur, G. Weiss, and S. Hunklinger, Phys. Lett. A **132**, 55 (1988).
[32] H. Gleiter, Adv. Mater. **4**, 474 (1992).

[33] A. Amirav, U. Even, and J. Jortner, J. Chem. Phys. **75**, 2489 (1981).
[34] S. Leutwyler, U. Even, and J. Jortner, J. Chem. Phys. **79**, 5769 (1983).
[35] N. Ben-Horin, U. Even, and J. Jortner, J. Chem. Phys. **97**, 5296 (1992).
[36] N. Ben-Horin, D. Bahatt, U. Even, and J. Jortner, J. Chem. Phys. **97**, 6011 (1992).
[37] S. Leutwyler and J. Bösiger, Faraday Discuss. Chem. Soc. **86**, 6011 (1988).
[38] L. Kador and P. Geissinger, Mol. Cryst. Liq. Cryst. **252**, 213 (1994).
[39] M. S. Anderson and C. S. Swenson, J. Phys. Chem. Solids **36**, 145 (1975).
[40] W. Schulze and D. M. Kolb, J. Chem. Soc. Faraday Trans. **70**, 1093 (1973).
[41] N. Steinmetz, H. Menges, J. Dutzi, and H. v. Löhneysen, Phys. Rev. B **39**, 2838 (1989).
[42] P. Geissinger, Ph.D. thesis, University of Bayreuth, 1994.